

## THREE-DIMENSIONAL HYDRODYNAMICAL SIMULATIONS OF STELLAR COLLISIONS. II. WHITE DWARFS

W. BENZ

Harvard-Smithsonian Center for Astrophysics

J. G. HILLS

Theoretical Division, Los Alamos National Laboratory

AND

F.-K. THIELEMANN

Harvard-Smithsonian Center for Astrophysics

Received 1988 October 28; accepted 1988 December 15

### ABSTRACT

We made three-dimensional numerical simulations of collisions between white dwarfs using a smooth particle hydrodynamics (SPH) code with 5000 particles. The code allows for radiation and degenerate pressure and uses a reduced nuclear network which models the large release of nuclear energy. Two different collision models are considered over a range of impact parameters: between two  $0.6 M_{\odot}$  carbon-oxygen white-dwarfs and between  $0.9 M_{\odot}$  and  $0.7 M_{\odot}$  carbon-oxygen white dwarfs. In nearly head-on collisions a very substantial fraction of the mass is lost as a result of a large release of nuclear energy. In grazing collisions, where nuclear energy release is much less important, the fraction of mass lost is close to that produced in collisions between main-sequence stars. The quantity of processed elements ejected into the interstellar medium by these collisions does not significantly affect the chemical evolution of the Galaxy. Some grazing collisions produce a coalescence of the two white dwarfs into an object whose mass exceeds the Chandrasekhar limit. The inevitable collapse of this white dwarf is delayed by the high temperature and fast rotation it acquired in the collision.

*Subject headings:* hydrodynamics — stars: interiors — stars: mass loss — stars: white dwarfs

### I. INTRODUCTION

Collisions between main-sequence stars are important in the cores of globular clusters (Hills and Day 1976) and in galactic nuclei. White dwarfs, being the end product of the evolution of most stars, should coexist in large numbers with main-sequence stars in these systems. We expect collisions in which one of the colliding stars is a compact object to be relatively frequent. Unfortunately, computer simulations of collisions between a white dwarf and a giant or between a white dwarf and a main-sequence star are exceptionally challenging because of the huge differences in densities and dimensions between these stars. Shara and Shaviv (1977, 1978), Shara and Regev (1986), and Regev and Shara (1987) attempted to simulate head-on collisions between main-sequence stars of various masses and a white dwarf (modeled as a point mass) in two dimensions using a very rudimentary scheme to model nuclear energy release. Simulations in three-dimensions of encounters between a low-mass main-sequence star and a white dwarf have been published recently by Soker *et al.* (1987). They show that for a wide range of off-axis collisions the encounter resulted in the formation of a massive disk around the white dwarf. The formation of such disks was also obtained by Benz and Hills (1987, hereafter Paper I) in their simulations of main-sequence star collisions. We show in this paper that they also form in collisions of two white dwarfs.

In this paper, which is the second step in the learning curve towards the simulation of collisions between main-sequence stars and compact objects, we investigate collisions between two white dwarfs. These collisions may seem quite unlikely since white dwarfs are about one to two orders-of-magnitude smaller than the lower main-sequence stars found in older

stellar systems. However, the cross sections for collisions are proportional to the product of the sum of the masses of the colliding stars and the sum of their radii because gravitational focusing dominates (Hills and Day 1976), so the collision cross section for two white dwarfs is about equal to that between two  $0.1 M_{\odot}$  main-sequence stars and is about two order-of-magnitude smaller than that for collisions between two main-sequence stars with masses of  $1 M_{\odot}$ . In the last section of this paper we compute the probability of a collision between two white dwarfs in the core of a typical globular cluster and in the Galactic center. These statistical calculations show that white-dwarf collisions do occur in these dense stellar systems.

The study of collisions between two white dwarfs requires additional physics not needed in studies of collisions between main-sequence stars, such as the production of a large amount of nuclear energy during the collision and the effect of radiation pressure. Comparisons between the results of white-dwarf and main-sequence star collisions can be used to better identify which physics is primarily responsible for producing a given property of the collisions. Much of the nuclear-processed material in white-dwarf collisions is ejected into the interstellar medium where it may be detectable. Furthermore, a collision can produce a white dwarf more massive than the Chandrasekhar limit whose existence is eventually announced by the subsequent Type I supernova. Supernovae occurring in the nuclei of galaxies, such as S Andromedae, SN 1885, which appeared in the nucleus of M31, may be suspected to be collision-induced events.

In § II we describe the set of equations that are solved in simulating the collisions while in § III we focus on the nuclear network we developed to take into account the large amount

of nuclear energy generated in some of the white-dwarf collisions. Section IV is a brief summary of our smooth particle hydrodynamics (SPH) code. Sections V and VI present the results of the simulations, whereas in § VII we compute collision rates and discuss various implications of these collisions.

## II. EVOLUTION EQUATIONS

Our calculations ignore radiation transport, which is a reasonable simplification. Except for a very small fraction of the total mass in the outer atmosphere of the stars (which is not modeled by the code), essentially all shocks occur in optically thick regions where heat is transported on diffusion time scales which much exceed the shock crossing time. We ignore complications such as magnetic fields.

In our previous paper on main-sequence star collisions (Paper I), we neglected nuclear energy release because the time during which the temperature exceeded hydrogen ignition threshold was too short for any significant generation of energy. The situation is quite different for colliding white dwarfs. These stars are composed of helium or carbon-oxygen, and their nuclear ignition takes place in the degenerate regime. As we will show, the temperature in the shock easily reaches carbon ignition threshold, so we include in our hydro code a small nuclear network that will be described in § III.

The results reported below were obtained using a fully three-dimensional hydrodynamic code which includes self-gravity and makes no assumptions about the flow symmetry. The hydrodynamics is described by the momentum equation in its Lagrangian form:

$$\frac{dv}{dt} = -\frac{\nabla P_{\text{tot}}}{\rho} - \nabla\phi + \mathbf{S}_{\text{visc}} \quad (2.1)$$

where  $\mathbf{S}_{\text{visc}}$  is the classical artificial viscous stress which is introduced to model kinetic energy dissipation in shocks; and the gravitational potential  $\phi$  is obtained from Poisson's equation

$$\nabla^2\phi = 4\pi G\rho. \quad (2.2)$$

The mass density is denoted by  $\rho$ , the gravitational constant by  $G$ , and  $\mathbf{v}$  is the velocity of a mass element. The total fluid pressure consists of a degenerate electron pressure, a nondegenerate gas pressure, and a radiation pressure term:

$$P_{\text{tot}} = P_{\text{deg}} + P_{\text{gas}} + P_{\text{rad}}. \quad (2.3)$$

In the degenerate regime, the pressure is obtained from the ideal, fully relativistic equation of state (Chandrasekhar 1939):

$$P_{\text{deg}} = Af(x);$$

$$f(x) = [x(2x^2 - 3)(x^2 + 1)^{1/2} + 3 \log(x^2 + 1)^{1/2}];$$

$$\rho = Bx^3; \quad (2.4)$$

where  $P_{\text{deg}}$  is the pressure,  $\rho$  is the density,  $A = 6.01 \times 10^{22}$ , and  $B = 9.82 \times 10^5 \mu_e$ . The mean molecular weight per electron  $\mu_e$  is updated as the simulation proceeds and the abundances of the element changes due to nuclear burning. The corresponding specific internal energy is given by the expression:

$$U_{\text{deg}} = \frac{Ag(x)}{\rho}, \quad g(x) = 8x^3[(x^2 + 1)^{1/2} - 1] - f(x). \quad (2.5)$$

The gas pressure is described by the nondegenerate equation of state

$$P_{\text{gas}} = (\gamma - 1)\rho U_{\text{therm}} \quad (2.6)$$

with  $\gamma = 5/3$ .

The radiation pressure term has the usual form:

$$P_{\text{rad}} = \frac{1}{3}aT^4. \quad (2.7)$$

The variation of the total specific internal energy  $U_{\text{tot}}$  is given by the first law of thermodynamics:

$$\frac{dU_{\text{tot}}}{dt} = -P_{\text{tot}} \frac{dV}{dt} + \frac{dQ}{dt}, \quad (2.8)$$

where  $V$  is the volume and  $dQ$  is the heat generated by the dissipation of kinetic energy in shocks and is related to the artificial viscous stress. All other energy sources, besides nuclear energy generation (see § III), have been neglected.

The gas pressure  $P_{\text{gas}}$  and the radiation pressure are found by first computing the nondegenerate part of the specific internal energy:

$$U_{\text{nondeg}} = U_{\text{tot}} - U_{\text{deg}}, \quad (2.9)$$

where  $U_{\text{deg}}$  is given by equation (2.5). This  $U_{\text{nondeg}}$  energy is then set equal to the sum of radiation energy plus the thermal energy. We therefore write:

$$U_{\text{nondeg}} = U_{\text{rad}} + U_{\text{therm}} = aT^4 + c_v T, \quad (2.10)$$

where  $c_v$  is the specific heat at constant volume. We solve equation (2.10) for  $T$ . Once  $T$  is known, the radiation and thermal components of the specific energy and the pressure can be readily computed.

The mass continuity equation is trivially incorporated by the numerical algorithm which is described in § IV.

Equations (2.1)–(2.10) represent a closed system that can be solved for the time evolution of the system once the initial state has been specified.

## III. THE NUCLEAR NETWORK

The high temperatures reached during the collision requires that nuclear energy release be included in the code. Unfortunately, a full nuclear network coupled to a three-dimensional hydro code would take a prohibitively large amount of computer time and storage. We devised a reduced nuclear network which meets the needs of these calculations: we are interested in the dynamics of the collision rather than in the detailed chemical composition of the material, so our network needs only to reproduce the energy generation accurately. This energy release must take place over the correct time scale. The bulk composition of white dwarfs is generally a mixture of carbon and oxygen. For He white dwarfs helium must also to be considered. Proton-induced reactions can largely be neglected.

The above considerations led us to include the following elements in our network:  ${}^4\text{He}$ ,  ${}^{12}\text{C}$ ,  ${}^{16}\text{O}$ ,  ${}^{20}\text{Ne}$ ,  ${}^{24}\text{Mg}$ ,  ${}^{28}\text{Si}$ ,  ${}^{32}\text{S}$ ,  ${}^{36}\text{Ar}$ ,  ${}^{40}\text{Ca}$ ,  ${}^{44}\text{Ti}$ ,  ${}^{48}\text{Cr}$ ,  ${}^{52}\text{Fe}$ ,  ${}^{56}\text{Ni}$ , and  ${}^{60}\text{Zn}$ . These nuclei cover all essential burning stages from helium burning on.

The individual reactions for various burning stages which are included in the network are discussed in the following papers:

*He-burning.*— ${}^4\text{He}(2\alpha, \gamma){}^{12}\text{C}$  and  ${}^{12}\text{C}(\alpha, \gamma){}^{16}\text{O}$  are taken from Nomoto, Thielemann, and Miyaji (1985) and Caughlan *et al.* (1985), respectively.

*C-burning.*—The employed  ${}^{12}\text{C}({}^{12}\text{C}, \alpha){}^{20}\text{Ne}$  rate is from Fowler, Caughlan, and Zimmerman (1975). In principle, this reaction has two channels, the alpha and the proton channel. However, most of the  ${}^{23}\text{Na}$  nuclei will react with the free protons via  ${}^{23}\text{Na}(p, \alpha){}^{20}\text{Ne}$  and “effectively” proceed through the alpha-channel. Therefore, we included only  ${}^{20}\text{Ne}$  as the

final product but with the reaction rate of the alpha + proton channel.

*Ne-burning.*—The main reactions are  $^{20}\text{Ne}(\gamma, \alpha)^{16}\text{O}$ , and  $^{20}\text{Ne}(\alpha, \gamma)^{24}\text{Mg}$  with rates from Fowler, Caughlan, and Zimmerman (1975) and  $^{24}\text{Mg}(\alpha, \gamma)^{28}\text{Si}$  from Harris *et al.* (1983).

*O-burning.*—The rate for oxygen fusion  $^{16}\text{O}(^{16}\text{O}, \alpha)^{28}\text{Si}$  is taken from Fowler, Caughlan, and Zimmerman (1975). As in carbon burning, we suppressed the proton channel to  $^{31}\text{P}$ , because in most cases it is followed by a (p,  $\alpha$ ) reaction to  $^{28}\text{Si}$ , which again can be handled as an “effective” alpha channel. Therefore, we used a rate for the alpha channel which results from the sum of both channels. The network also included the reaction  $^{16}\text{O}(^{12}\text{C}, \alpha)^{24}\text{Mg}$  by Hulke, Rolfs, and Trautvetter (1980), which can be important in explosive combined oxygen and carbon burning.

*Si-burning and nuclear statistical equilibrium.*—Si-burning is usually initiated by photodisintegration reactions at temperatures in excess of  $3 \times 10^9$  K, which provide the particles for capture reactions, and it ends in an equilibrium abundance distribution around Fe (thermodynamic equilibrium). A small energy generation network like the one employed here cannot contain all reactions involved. We want to concentrate on nuclei with major abundances. In an astrophysical plasma which starts with a distribution of nuclei with equal neutron and proton numbers ( $N = Z$ , like all nuclei mentioned above) and which does not allow for extensive electron capture and beta-decay due to a short burning time scale, the resulting abundance distribution will again be centered around a line of  $N = Z$ . Here the nuclei with even proton numbers have the larger binding energies and therefore the major abundance. For that reason, an alpha chain of nuclei starting at  $^{28}\text{Si}$  and ending beyond  $Z = 26$  can serve the purpose of an equilibrium network, which approximates the major abundances and energy generation. The doubly magic  $^{56}\text{Ni}$  nucleus plays a dominant role. All reaction rates in this alpha chain were calculated with the code SMOKER (see Thielemann, Arnould, and Truran 1987). Because a network like this does not contain neutron and proton captures it can underestimate the time scale for burning Si to Ni. In the approach to equilibrium with free neutrons and protons present, a combination of neutron and proton captures will be faster than alpha-induced reactions. Therefore, in intermediate temperature conditions in which Si and heavier nuclei are produced but no nuclear equilibrium is reached yet, Si could be overestimated. However, as the dominant energy release occurs from the transformation of C and O to Si, the energy generation and resulting effects on the hydrodynamics will be almost unaffected by this uncertainty.

The nuclear reaction rates, listed above, are generally denoted by  $\langle j, k \rangle := \langle \sigma v \rangle_{j,k}$  for a reaction between particles  $j$  and  $k$ , where the cross section is averaged over a Maxwell-Boltzmann distribution of relative velocities. In an application like the present one, where the astrophysical plasma has relatively high densities and is at least partially degenerate, effects of electron screening become highly important. Under most conditions the generalized reaction rate integral can be separated into the traditional expression without screening and a screening factor (see also Thielemann and Truran 1987)

$$\langle j, k \rangle^* = f_{\text{scr}}(Z_j, Z_k, \rho, T, Y_i) \langle j, k \rangle. \quad (3.1)$$

This screening factor is dependent on the charge of the involved particles, the density, temperature, and the composition of the plasma. Here  $Y_i$  denotes the abundance of nucleus  $i$

given by  $Y_i = n_i/(\rho N_A)$ , where  $n_i$  is the number density of nuclei per volume. In the present calculations we employed the description of Itoh *et al.* (1979, 1980) for the screening factors in the strong screening regime.

The reaction network is described by the following set of differential equations:

$$\dot{Y}_i = \sum_j c_j^i Y_j + \sum_{j,k} c_{j,k}^i Y_j Y_k + \sum_{j,k,l} c_{j,k,l}^i Y_j Y_k Y_l. \quad (3.2)$$

The coefficients  $c^i$  are connected with the reaction rates for (1) decays or photodisintegrations  $\lambda_j$ , (2) two-particle reactions  $\langle j, k \rangle$ , and (3) three-particle reactions  $\langle j, k, l \rangle$  like the triple-alpha process which can be interpreted as successive captures with an intermediate unstable target (see Nomoto, Thielemann, and Miyaji 1985). The individual  $c^i$ 's are given by  $c_j^i = N_i \lambda_j$ ,  $c_{j,k}^i = \rho N_A N_i / (N_j! N_k!) \langle j, k \rangle$ , and  $c_{j,k,l}^i = (\rho N_A)^2 N_i / (N_j! N_k! N_l!) \langle j, k, l \rangle$ . The  $N_i$ 's can be positive or negative numbers and specify how many particles of species  $i$  are created or destroyed in a reaction and the denominators including factorials avoid double counting of the number of reactions when identical particles react with each other (for example in the  $^{12}\text{C} + ^{12}\text{C}$  or the triple-alpha reaction; for details see Fowler, Caughlan, and Zimmermann 1967).

Equation (3.2) is solved with a first-order scheme (i.e., the Euler backward differentiation method where the right side is evaluated at the new grid point in time). The set of nonlinear equations resulting from this discretization is solved with the aid of a multidimensional Newton-Raphson iteration until an accuracy of  $10^{-7}$  is obtained. The total energy generation per gram due to nuclear reactions in a time step  $\delta t_{\text{nuc}}$  which changed the abundance by  $\delta Y_i$  is given by

$$\delta \epsilon = - \sum_i \delta Y_i N_A M_{\text{ex},i} c^2 \quad (3.3)$$

where  $M_{\text{ex},i}$  denotes the mass excess of nucleus  $i$ . The time step is determined by

$$\delta t_{\text{nuc}} = 0.1 \text{ min}_i \left[ \frac{Y_i(t)}{Y_i(t) - Y_i(t - \delta t_{\text{nuc},\text{old}})} \right] \delta t_{\text{nuc},\text{old}} \quad (3.4)$$

where the minimum is taken only for nuclei with an abundance in excess of  $10^{-7}$ .

#### IV. NUMERICAL TECHNIQUES

To solve the system of equations outlined in § II in three dimensions, we use, as in Paper I, the smooth particle hydrodynamics method (SPH). This method has been described extensively in the literature as have a number of tests to check its ability to reproduce analytical and experimental results (see, for example, Monaghan 1985; Benz 1988 and references therein). SPH is a free Lagrangian method for solving the conservation equations of hydrodynamics in which a finite set of extended Lagrangian particles replaces the continuum of hydrodynamic variables. The finite extent of the Lagrangian particles is determined by a smoothing function (or kernel) containing a characteristic length scale  $h$ . This length scale is roughly analogous to a zoning scale in conventional finite difference methods. In this paper we use the kernel called  $W_4$  in Monaghan and Lattanzio (1985) which is based on  $B$ -splines rather than the exponential kernel used in Paper I. This kernel has a number of advantages over the exponential kernel (Monaghan 1985). The advantage of SPH is that the usual mesh upon which traditional finite difference methods are based is not needed, so SPH does not suffer from mesh tan-

gling or inaccuracies associated with the severe distortion of the mesh. SPH is particularly suited for the simulation of highly distorted flows such as those occurring during impacts. Compared to Eulerian schemes, SPH is also particularly advantageous where large voids have to be modeled, as is the case in this problem. No computer memory or time is wasted by having a large number of empty cells just in case some material moves into them. A typical simulation is evolved in time by computing the trajectories of all particles from the various forces acting among them. These forces are computed from the interactions between the particles that depend on their relative positions and velocities.

The most expensive part of the calculation is the determination of the gravitational force. We use the hierarchical binary tree to determine the gravitational potential and force that has been described in Benz *et al.* (1989). In this method a tree (really an inverted tree) is constructed from the particles; the tree has a hierarchical structure of nodes. The particles themselves are at the lowest layer of nodes, the leaves. The next layer of nodes is constructed from those particle pairs consisting of mutual nearest neighbors; the node is located at the center of mass of the pair, and the quadrupole moment of the pair is computed. The computation of the rest of the tree proceeds in an analogous fashion. In each case, mutual nearest neighbor nodes or particles or particle-nodes are merged into a node for which the center of mass and quadrupole moments are computed. Eventually, there is just one node at the top of the tree. Clearly, when computing the forces on a particle, a node far away from it need not be expanded but can be used as is with its quadrupole moment correction; the desired degree of accuracy dictates how far the tree must be expanded in the gravitational force calculation for any given particle. The computational cost of this algorithm scales as  $N \log N$  for large  $N$ . The same tree can easily be used to find all the neighbors of any given particle that contributes to the local properties (density, pressure, and so on).

Each particle is described by the following quantities: mass, specific internal energy, chemical composition and position in phase space. As in traditional Lagrangian hydrodynamics, the mass of the particle is constant in time (but all particles need not be equally massive). We use operator splitting to treat the hydrodynamics and the nuclear burning. First, a hydro time step is computed in which the hydrodynamic equations and equation (2.10) are solved for each particle. At the end of the hydro time step, the position, velocity, density, and internal energy of each particle are updated. Next, we use our nuclear network to compute the nuclear energy that was released during the hydro time step. The nuclear time step used (eq. [3.4]) is, on average,  $\sim 2-4$  times smaller than the hydro time step, but can be much smaller during very violent nuclear burning. At the end of this part of the code the particle's chemical composition is updated and the total nuclear energy release is added to the internal energy of the particle under consideration and the system is ready for the next hydro time step.

#### V. INITIAL CONDITIONS

Paper I showed that the results of a collision between two stars are nearly independent of their relative velocity if it is less than their surface escape velocity. For an  $0.5 M_{\odot}$  white dwarf the escape velocity is  $\sim 4000 \text{ km s}^{-1}$ . This velocity is more than one order of magnitude larger than the velocity dispersion of stars in galactic nuclei and nearly three orders of magnitude larger than the velocity dispersion of stars in globular

clusters. This greatly reduces the initial conditions parameter space we have to consider. We compute only collisions for which the relative velocity at infinity is zero.

Having specified the initial relative velocity, we need to specify several more parameters before starting the simulations including individual masses, density structure, chemical composition, and impact parameter. To keep the number of simulations within reasonable bounds, we only simulated collisions between two  $0.6 M_{\odot}$  and between an  $0.7 M_{\odot}$  and an  $0.9 M_{\odot}$  white dwarf. We assume the precollision stars are zero-temperature, completely degenerate white dwarfs. The internal pressure and specific energy are given by equations (2.4) and (2.5), respectively, so that the internal structure of the stars is completely determined once the chemical composition is specified. This assumption is not critical since the energy released in shocks in head-on collisions far exceeds any reasonable initial energy that we might choose. For grazing collisions, gravitational torques are responsible for the mass loss. They will be shown to be quite insensitive to the internal structure of the stars. Finally, we specify that all our white dwarfs are composed of an homogenized mixture of 50% carbon and 50% oxygen. All the simulations reported in this paper have been performed using 5000 particles.

With the above choice we have performed two sets of simulations, one between two  $0.6 M_{\odot}$  white dwarfs and one between an  $0.7 M_{\odot}$  and an  $0.9 M_{\odot}$  white dwarf. For each set of simulations we have varied the impact parameter so that the various collisions range from head-on to grazing. For each collision we have determined the amount and chemical composition of the ejected mass as well as the amount of mass in the merged object and any accretion disk around it. The initial conditions for the simulations and their general results are given in Table 1.

#### VI. RESULTS

We describe the individual collisions in this section, while in the next one we give the collision cross sections and global properties such as the enrichment of the interstellar medium due to the ejection of processed elements. We recall that in all the collisions we took the impact velocity of the two stars at infinity to be zero (see discussion in § II).

The overall results are given in the first seven rows of Table 1. Columns (1) and (2) give the masses of the colliding stars. Column (3) gives  $R_{\min}$ , the minimum separation of the two

TABLE 1  
SUMMARY OF COLLISION RESULTS

| Run<br>(1) | $M_1$<br>( $M_{\odot}$ )<br>(2) | $M_2$<br>( $M_{\odot}$ )<br>(3) | $\frac{R_{\min}}{R_1 + R_2}$<br>(4) | $M_{\text{lost}}$<br>( $M_{\odot}$ )<br>(5) | $M_{\text{bound}}$<br>( $M_{\odot}$ )<br>(6) | $M_{\text{disk}}$<br>( $M_{\odot}$ )<br>(7) |
|------------|---------------------------------|---------------------------------|-------------------------------------|---|--|---|
| 1.....     | 0.6                             | 0.6                             | 0.000                               | 0.09  | 1.11   | 0.00  |
| 2.....     | 0.6                             | 0.6                             | 0.166                               | 0.05  | 1.15   | 0.00  |
| 3.....     | 0.6                             | 0.6                             | 0.282                               | 0.02  | 1.18   | 0.00  |
| 4.....     | 0.6                             | 0.6                             | 0.507                               | 0.03  | 1.12   | 0.05  |
| 5.....     | 0.6                             | 0.6                             | 0.705                               | 0.05  | 1.05   | 0.10  |
| 6.....     | 0.6                             | 0.6                             | 0.772                               | 0.05  | 1.04   | 0.11  |
| 7.....     | 0.6                             | 0.6                             | 0.970                               | 0.00  | binary                                       | 0.00  |
| 8.....     | 0.9                             | 0.7                             | 0.000                               | 0.57  | 1.03   | 0.00  |
| 9.....     | 0.9                             | 0.7                             | 0.014                               | 0.52  | 1.08   | 0.00  |
| 10.....    | 0.9                             | 0.7                             | 0.243                               | 0.08  | 1.52   | 0.00  |
| 11.....    | 0.9                             | 0.7                             | 0.464                               | 0.05  | 1.55   | 0.00  |
| 12.....    | 0.9                             | 0.7                             | 0.696                               | 0.06  | 1.42   | 0.12  |
| 13.....    | 0.9                             | 0.7                             | 0.955                               | 0.10  | 1.41   | 0.09  |

stars in the encounter if they were point masses, in units of the sum of their radii  $R_1 + R_2$ ;  $R_{\min}$  was calculated analytically from the preencounter orbital angular momentum and kinetic energy. The amount of mass lost from the system (in solar masses) is given in column (4). This mass loss was computed in the same manner as in Paper I. Columns (5) and (6) give, respectively, the mass of the merged object and the mass of any accretion disk orbiting it.

Figure 1 shows the fraction of mass lost plotted as a function of  $R_{\min}$  for the two series of white dwarf collisions calculated in this paper and for main-sequence collisions with impact velocity  $V = 0$ , which were computed in Paper I. Figure 2 shows the mass of the accretion disk as a function of  $R_{\min}$  for these three series of collisions. We note that the amount of mass loss and the mass of the accretion disk increase in grazing collisions for all three series of collisions. This is due to gravitational torquing of each star by the other and the large amount of angular momentum in the coalesced objects. Jetting produces the local maximum in the mass lost at zero impact parameter. It is greater for the collisions between the more massive white dwarfs because of the large amount of nuclear energy released.

As in Paper I, we can only summarize a small fraction of the tremendous amount of detail shown in these simulations. We try to give the flavor of these collisions by illustrating them with a selection of representative cases which are discussed below.

#### i) Collisions between $0.6 M_{\odot}$ White dwarfs

We simulated seven collisions between two  $0.6 M_{\odot}$  white dwarfs. Their global results are listed in the first seven lines of Table 1.

Figure 3 gives snapshots of the stars during a head-on collision. We notice the high-speed jets which form in the collision plane during the initial contact and the rebound of material

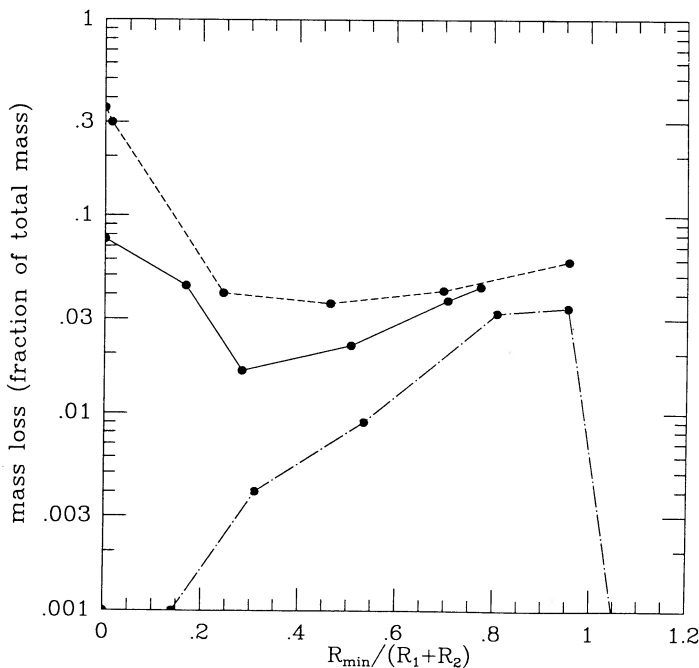


FIG. 1.—Fraction of the mass of the two stars lost in a collision plotted as a function of their closest approach in units of the sum of their radii. Plots are given for collisions between two white dwarfs with masses of  $0.6 M_{\odot}$  each (solid line), two white dwarfs with masses of  $0.7$  and  $0.9 M_{\odot}$  (dashed line), and two equally massive lower main-sequence stars (dash-dotted line).

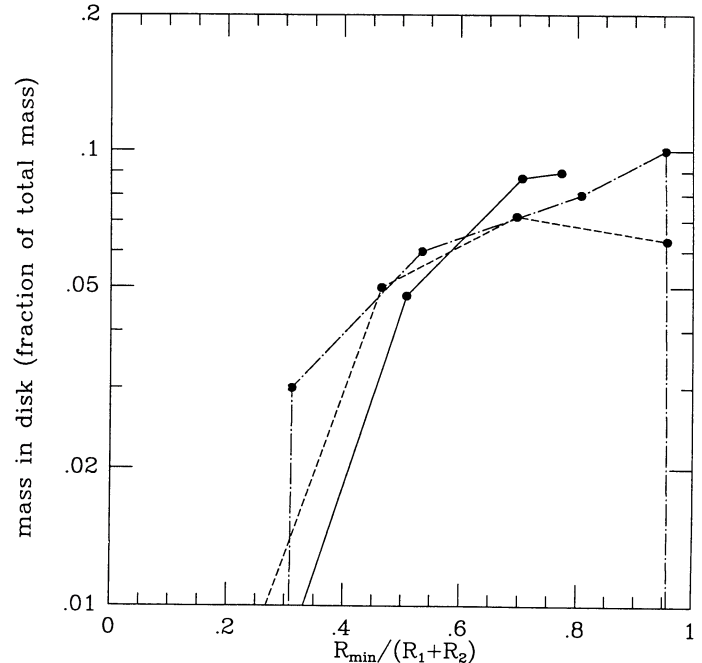


FIG. 2.—The fraction of the mass of the two colliding stars which ends up in an accretion disk around the final coalesced star. This is for the same three series of calculations given in Fig. 1, and the line types have the same meaning.

perpendicular to this plane which occurs after the shock propagates through the stars. Both these phenomena produce mass loss. This superelastic rebound is especially vigorous because of the high temperature reached in the shock due to the production of significant nuclear energy.

Figure 4 shows for this simulation the variation in time of the various specific energies. We note the increase in kinetic energy as the two stars approach each other. When they collide, the thermal energy increases sharply due to the rapid release of nuclear energy. From the variations in the potential energy we see that the coalesced object oscillates with a period of  $\sim 15$  s. As found for main-sequence collisions given in Paper I, these oscillations are slowly damped as the object settles to dynamical equilibrium. From this figure, we notice that the total nuclear energy release in the collision is about a third of the initial thermal energy in the stars. This additional energy causes the fraction of mass loss to be much larger than that found in head-on collision between two equal-mass main-sequence stars (see Paper I) for which nuclear-energy production is negligible.

Figure 5 shows the fractional abundance of the chemical elements in the ejecta for all simulations of  $0.6 M_{\odot}$  collisions plotted as a function of the closest approach,  $R_{\min}$ . We find that in a head-on collision the mass fraction of carbon goes from 0.5 to 0.353 and oxygen from 0.5 to 0.387. The major heavy elements produced are  $^{24}\text{Mg}$  (0.01443),  $^{28}\text{Si}$  (0.0846),  $^{32}\text{S}$  (0.0447), and  $^{56}\text{Ni}$  (0.0881). All other elements are present with mass fractions less than 0.005. Since  $0.09 M_{\odot}$  have been lost in the collision,  $\sim 0.0076 M_{\odot}$  of  $^{28}\text{Si}$  and  $0.0079 M_{\odot}$  of  $^{56}\text{Ni}$  are ejected into the interstellar medium for each head-on collision between two  $0.6 M_{\odot}$  white dwarfs. The extent to which this ejecta enriches the interstellar medium in heavy elements is estimated in the next section.

Increasing  $R_{\min}/(R_1 + R_2)$  to 0.166 (simulation 2) decreases the mass lost from the system because the shock weakens con-

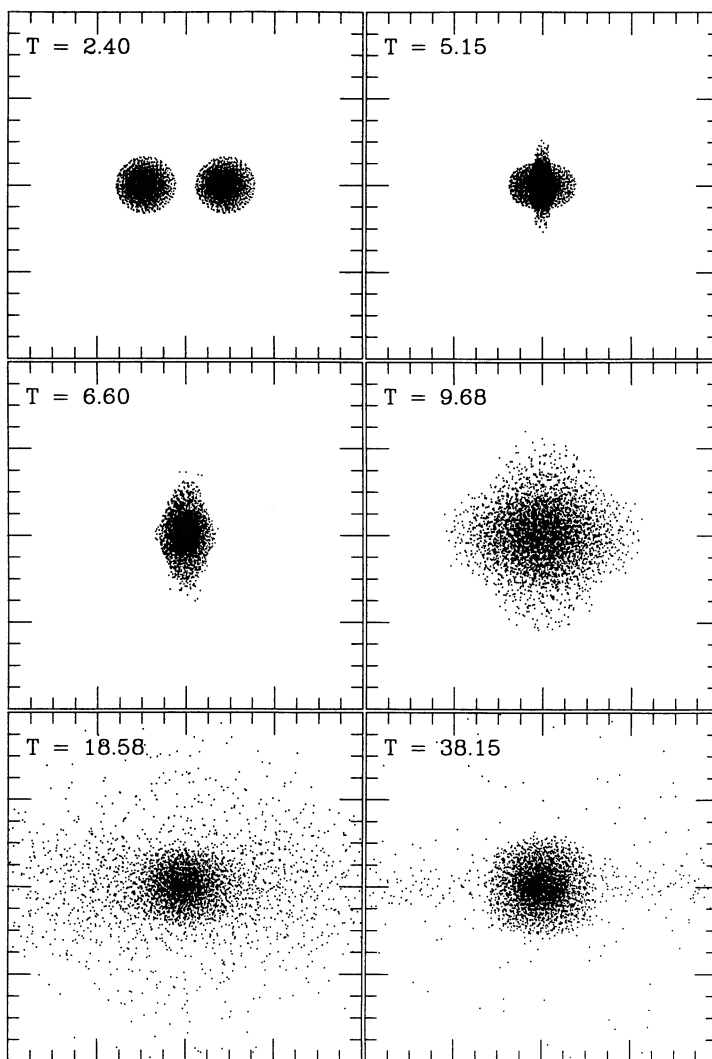


FIG. 3.—Projections onto the plane of the initial orbit of the fluid particles in two colliding white dwarfs at various times during a head-on collision (simulation 1). The times are measured in seconds from the beginning of the simulation. Each frame of the figure covers a spatial region of  $8 \times 10^9$  cm by  $8 \times 10^9$  cm.

siderably. The temperature and density in the shock do not increase as much as in the head-on collision, so less nuclear energy is released. This is illustrated by the relative abundances of the elements produced in the collision. From Figure 5 we find that although  $^{28}\text{Si}$  is slightly more abundant (0.115) considerably less  $^{56}\text{Ni}$  is produced (0.0399). The total mass ejected is  $0.0058 M_{\odot}$  of  $^{28}\text{Si}$  and  $0.002 M_{\odot}$  of  $^{56}\text{Ni}$  which for both elements is significantly less than in the head-on collision.

Increasing  $R_{\min}/(R_1 + R_2)$  to 0.282 (simulation 3) leads to a further sharp decrease in the mass loss. This collision produces the smallest mass loss found in any of the simulations reported here (see Fig. 1). Figure 6, which shows pictures made at selected times during the collision, indicates that the merging of the two stars is a two-step process. The two stars survive the initial impact, but they lose kinetic energy. As they move away from each other, their self-gravity slows down their velocity of recession. Because of the energy dissipation in the collision, the two stars do not recede very far from each other before turning around and colliding again. During this collision they form a bar-like structure which redistributes the angular momentum as they roll around each other, so they finally merge into one

object. This scenario is typical of collisions at large enough impact parameters. The only feature that varies is the number of closest approaches needed to dissipate enough kinetic energy to allow the final merger. In this simulation one close encounter was sufficient. We have found that up to three pericenter passages are needed in grazing collisions before a merger occurs. The evolution of the various energies during the collision shown in Figure 6 is displayed in Figure 7. We note that little nuclear energy was generated during the collision. The figure shows that the mutual perturbations of the stars cause them to pulsate until their final merger into one object in dynamical equilibrium. Figure 5 shows that this simulation did not produce a significant quantity of heavy elements including  $^{56}\text{Ni}$ . In fact, except for the initial carbon and oxygen, the only other elements present in a significant fraction are  $^{28}\text{Si}$  (0.104) and  $^{24}\text{Mg}$  (0.043) which amount, respectively, to  $0.002 M_{\odot}$  of  $^{28}\text{Si}$  and  $0.00085 M_{\odot}$  of  $^{24}\text{Mg}$ .

If  $R_{\min}$  is larger than half the sum of the radii of the two stars no significant nuclear energy is released, and the ejecta have almost exactly the initial chemical composition. Only a few elements produced in nuclear reactions in the collision are

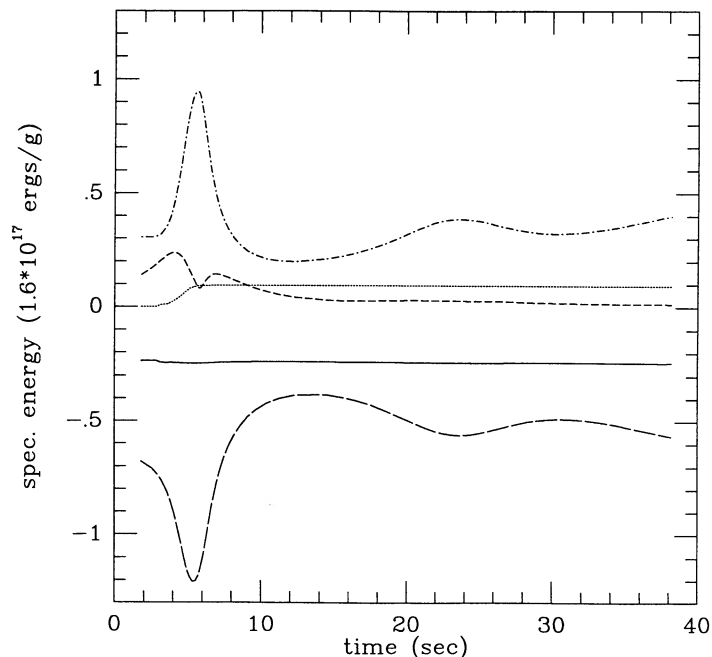


FIG. 4.—Time variations in the specific energies for the collision shown in Fig. 3: kinetic (short dashed line), thermal (dash-dotted line), potential (long dashed line), and total (solid line) as well as the total nuclear energy generated since the beginning of the simulation (dotted line). Time is again given in seconds, whereas the specific energies are given in units of  $1.6 \times 10^{17}$  ergs  $g^{-1}$ .

present and only as traces. At larger values of  $R_{\min}$ , the initial shock has no significant effect other than dissipating orbital kinetic energy so the semimajor axis of the orbit is reduced at each pericenter passage. As we found for main-sequence collisions in Paper I, in grazing collisions the shock does not play a significant role in mass loss. Mass is lost because the strong

gravitational torques transfer angular momentum outward causing the ejection of the outer parts of the merged object. A good example of this is found in simulation 6, for which  $R_{\min}/(R_1 + R_2) = 0.772$ . Figure 8 shows the time dependence of the various energies for this simulation. As a result of the first impact, the two stars oscillate in phase as they move away from each other. These oscillations slowly damp out before the second close encounter. This second close encounter did not produce the final merger of the two stars; a third one was necessary. Figure 9 shows selected snapshots of the evolution of the collision. We note the “bridge” of material connecting the two stars after the first encounter. As they move away this material eventually falls back onto the two stars. In the final merger, we note the appearance of the same kind of spiral structure that was found in Paper I. The material in the outer parts of the arms is lost. It is worthwhile noting that the fraction of mass lost during these grazing collisions is similar to that found for grazing collisions between equal-mass main-sequence stars. This is not surprising, since gravitational torques are responsible for the mass loss in both cases. The equation of state, while quite different in the case of white dwarfs, is only of secondary importance. We suspect that 4%–5% of the total mass of the two stars is typically lost in grazing collisions between two equal-mass stars with an initial density distribution which follows a polytrope of index  $n = 1.5$ . As found in Paper I, these grazing collisions also result in the formation of an accretion disk having a substantial mass. In the particular case of simulation 6, the total mass of the accretion disk is  $\sim 0.11 M_{\odot}$ . The structure of the merged object and the accretion disk is shown in Figure 10. This is a projection of the particle velocities onto a plane passing through the rotational axis of the merged object.

Finally, for  $R_{\min}/(R_1 + R_2) = 0.97$  (simulation 7) we found that no mass was lost but that the encounter resulted in the formation of a binary system. This result is quite different from

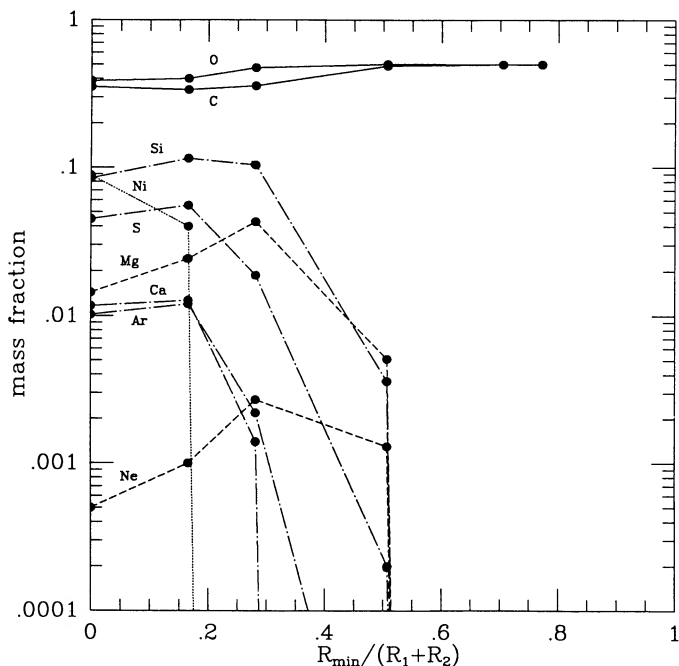


FIG. 5.—The fractional abundance of the chemical elements in the ejecta from collisions between two  $0.6 M_{\odot}$  white dwarfs. These data are plotted as a function of the closest approach in the orbit in units of sum of the radii of the two objects.

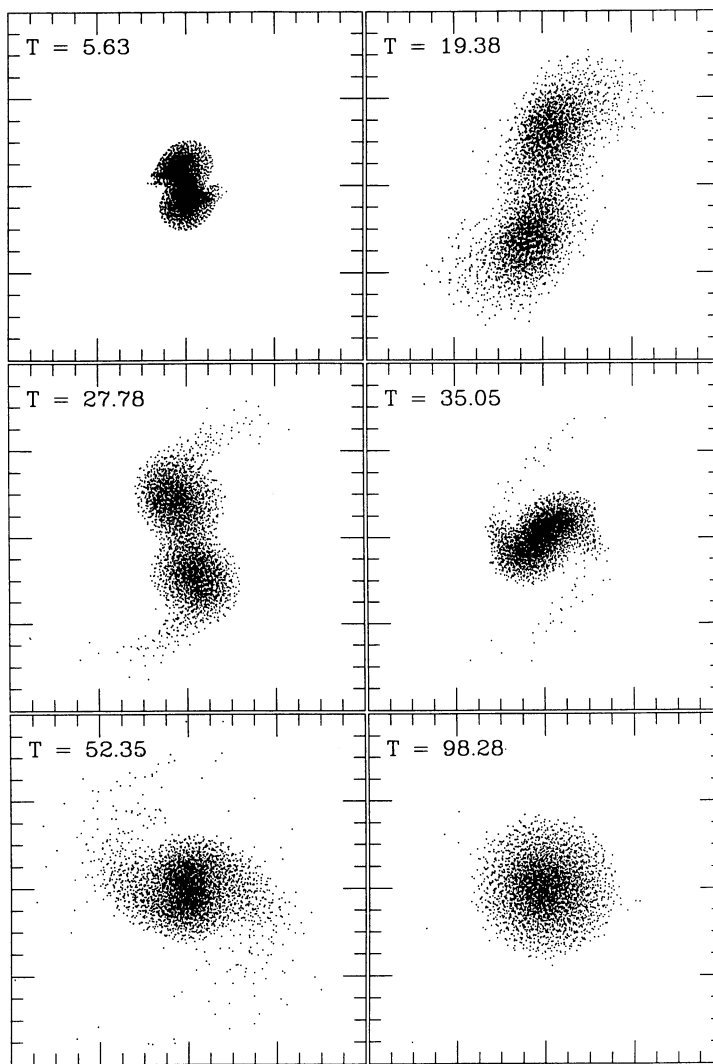


FIG. 6.—Projections onto the plane of the initial orbit of the fluid particles positions at various times during simulation 3, which involves a collision between two white dwarfs with masses of  $0.6 M_{\odot}$  each and with  $R_{\min}/(R_1 + R_2) = 0.282$ . As in Fig. 1, time is given in seconds, and each frame covers an area of  $8 \times 10^9$  cm by  $8 \times 10^9$  cm.

that found in low-velocity collisions between main-sequence stars where all encounters in which the two stars actually hit each other result in the merger of the two objects. We attribute this result to differences in equation of state between the two types of stars. For degenerate stars, pressure is independent of temperature, so the energy dissipated in the first collision can be absorbed by the stars without significantly increasing their radii. For nondegenerate stars, an increase in temperature always produces an increase in radius. Main-sequence stars produce a runaway situation where the energy dissipated during the first impact increases the radius so the two stars overlap slightly more on their second encounter which allows even more dissipation and in turn increases their radii and so on. We are presently running a number of simulations to investigate the possibility of forming double white dwarf binaries by tidal dissipation in close encounters, so we will delay any further discussion of these matters to a forthcoming paper.

ii) *Collisions between  $0.9 M_{\odot}$  and  $0.7 M_{\odot}$  White Dwarfs*

We present here, for the first time, a series of six simulations of collisions between two unequal mass stars. The results are

summarized starting on row 8 of Table 1. We will, in reporting the results, concentrate on the differences between these simulations and equal-mass star collisions. As we will see, these collisions are substantially more efficient in expelling mass and producing heavy elements for the same relative velocity at infinity. The kinetic energy per unit mass at impact is substantially greater in a collision between two massive white dwarfs than in a collision between two less massive ones, so the shock temperatures and the amount of nuclear energy release are much larger for the more massive white dwarfs.

From Figure 1, we notice the huge mass loss in a head-on collision. About 35% of the total mass or  $0.57 M_{\odot}$  is ejected from the system. Figure 11 shows the time variation of the various energies during a head-on collision. It is evident that the large mass loss results from the large amount of nuclear energy generated in the collision. In this collision the nuclear energy release is almost twice the initial internal energy of the stars. Figure 12 displays pictures made at selected times during this collision. We notice the sharp oblique shock at the interface between the two stars at the initial impact. Only the less massive and less dense star (the one with the larger radius) is

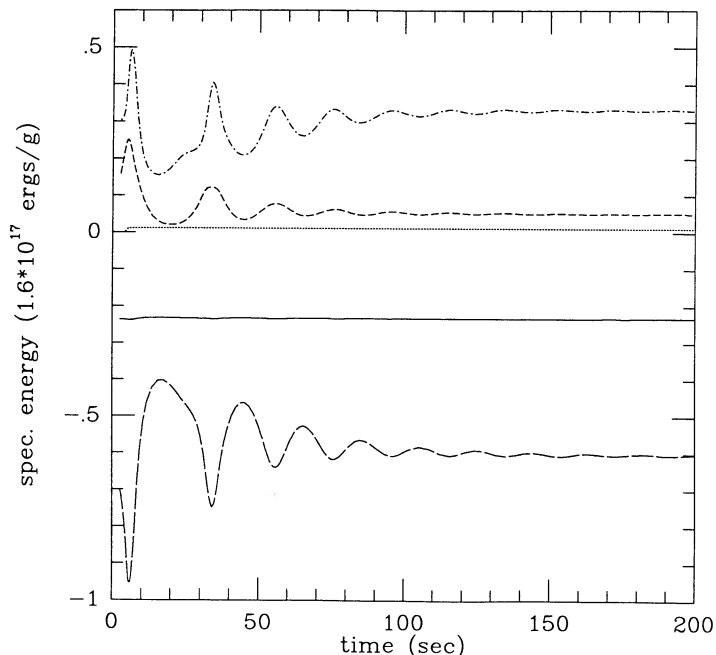


FIG. 7.—Time variations in the specific energies for the collision given in Fig. 6: kinetic (*short dashed line*), thermal (*dash-dotted line*), potential (*long dashed line*), and total (*solid line*) as well as the total nuclear energy generated since the beginning of the simulation (*dotted line*). Time is again in units of seconds whereas the specific energies are given in units of  $1.6 \times 10^{17}$  ergs  $g^{-1}$ .

destroyed. The more massive, denser star suffers only marginally from the collision, and, in fact, gains  $0.07 M_{\odot}$  from the collision. This behavior is due to the shock being much stronger in the less massive, less dense star, in which a detonation wave is generated that destroys it completely. We notice that the chemical composition of the ejecta is also quite remarkable,

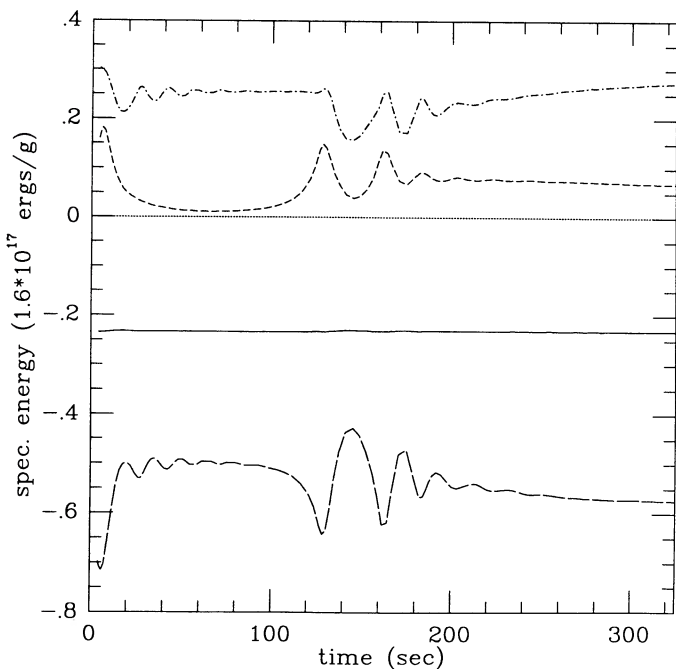


FIG. 8.—Time variations in the specific energies for the collision given in Fig. 9: kinetic (*short dashed line*), thermal (*dash-dotted line*), potential (*long dashed line*), and total (*solid line*) as well as the total nuclear energy generated since the beginning of the simulation (*dotted line*). Time is given in seconds, whereas the specific energies are given in units of  $1.6 \times 10^{17}$  ergs  $g^{-1}$ .

as shown in Figure 13. Besides the original carbon (now down to 0.179) and oxygen (now down to 0.214), it is composed mainly of  $^{56}\text{Ni}$  (0.297) and  $^{28}\text{Si}$  (0.130). This represents a total amount of  $0.17 M_{\odot}$  of  $^{56}\text{Ni}$  and  $0.074 M_{\odot}$  of  $^{28}\text{Si}$  that is ejected in the collision.

Increasing  $R_{\min}$  reduces the shock strength, so the maximum shock temperature is less, as is the mass loss and the nuclear energy generation. This trend was also found in cases where two equal-mass white dwarfs collide. A dramatic example of this sharp decrease in shock strength is illustrated by simulation 10, for which the closest approach  $R_{\min}$  is slightly below a quarter of the sum of the two radii. In this simulation the mass loss has already dropped to  $0.075 M_{\odot}$ , i.e., by more than a factor of 7 from the head-on collision! The amount of  $^{56}\text{Ni}$  ejected has decreased even more since its mass fraction in the ejecta has dropped below 0.1. However, the amount of processed elements ejected in this collision considerably exceeds that found in any collision between equal-mass white dwarfs.

#### VII. COLLISION RATES

We shall use the results of the previous section to compute cross sections for coalescence and mass loss. We follow the procedure used in Paper I, which was based on equations given in Hills and Day (1976). We use these cross sections to determine the rate of collisions among white dwarfs in globular clusters and the Galactic center.

In the limit where the stellar velocity dispersion is much less than the escape velocity from the surface of the colliding stars, which is the case for collisions among white dwarfs in globular clusters and the Galactic center, Paper I shows the ratio of the coalescence cross section to the geometric cross section,  $\sigma_0 = \pi(R_1 + R_2)^2$ , to be given by

$$\frac{\sigma_c}{\sigma_0} = \left( \frac{R_{\text{fusion}}}{R_1 + R_2} \right) \left( \frac{V_{\text{esc}}}{V} \right)^2. \quad (7.1)$$

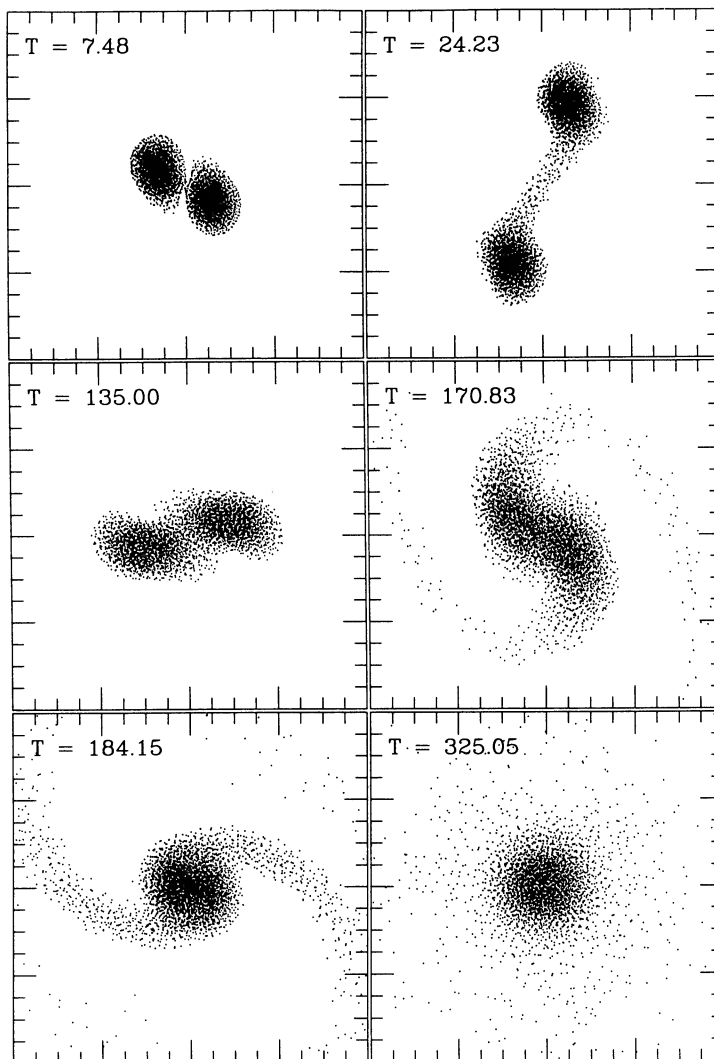


FIG. 9.—Projections onto the plane of the initial orbit of the fluid particles position at various times during simulation 6, which involves a collision between two white dwarfs with masses of  $0.6 M_{\odot}$  each and with  $R_{\min}/(R_1 + R_2) = 0.772$ . As in Fig. 1, time is given in seconds, and each frame covers an area of  $8 \times 10^9$  cm by  $8 \times 10^9$  cm.

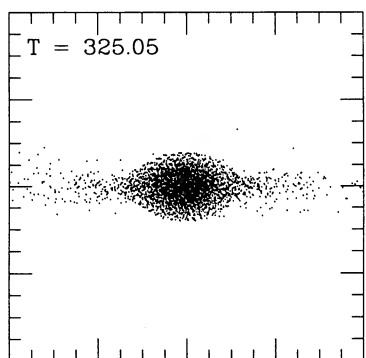


FIG. 10.—Projections of the fluid particles positions in the merged object which resulted from simulation 6. Projections are made onto a plane perpendicular to the original orbit. We note the fast rotation of the object and the accretion disk around it.

Here  $R_1$  and  $R_2$  are the radii of the two stars,  $V$  is the relative velocity of the two stars at infinity,  $R_{\text{fusion}}$  is the maximum value of  $R_{\min}$  which allows the coalescence of the two stars, and

$$V_{\text{esc}} = \left[ \frac{2G(M_1 + M_2)}{(R_1 + R_2)} \right]^{1/2}$$

is the escape velocity of the two stars when they are in contact with each other. Two colliding white dwarfs with masses of  $0.6 M_{\odot}$  and radii of  $0.0127 R_{\odot}$ , have an escape velocity of  $V_{\text{esc}} = 4240 \text{ km s}^{-1}$  at contact while two white dwarfs with masses of  $0.7$  and  $0.9 M_{\odot}$  and radii of  $0.0114$  and  $0.00924 R_{\odot}$ , respectively, have  $V_{\text{esc}} = 5440 \text{ km s}^{-1}$ .

Paper I also shows that coalescence occurs if  $R_{\min}/(R_1 + R_2) \leq 1.03$  for equal-mass main-sequence stars. We have fewer simulations of white dwarf collisions at nearly grazing

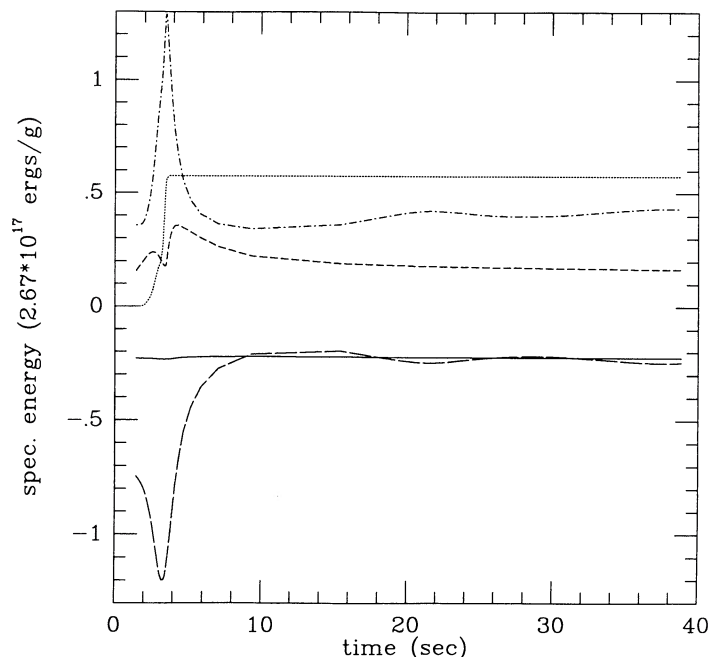


FIG. 11.—Time variations in the specific energies during simulation 8 which shows a head-on collision between a  $0.9 M_{\odot}$  white dwarf and a  $0.7 M_{\odot}$  one: kinetic (short dashed line), thermal (dash-dotted line), potential (long dashed line), and total (solid line) as well as the total nuclear energy generated since the beginning of the simulation (dotted line). Time is again given in seconds, whereas the specific energies are given in units of  $2.67 \times 10^{17}$  ergs  $g^{-1}$ .

encounters, but they are consistent with  $R_{\text{fusion}}/(R_1 + R_2) \cong 1$ . We find that a collision between two white dwarfs with mass  $0.6 M_{\odot}$  produces a binary system if  $R_{\text{min}}/(R_1 + R_2) = 0.97$ . A collision between two main-sequence stars at this value of  $R_{\text{min}}/(R_1 + R_2)$  produces a single coalesced star (Paper I). However, gravitational radiation will cause the white dwarfs in this binary to merge in much less than a Hubble time.

For a typical globular cluster and for the Galactic center the velocity dispersion is less than  $10 \text{ km s}^{-1}$  and  $150 \text{ km s}^{-1}$ , respectively, so the cross sections for coalescence are more than  $10^5$  times the geometric cross section in globular clusters and  $10^3$  times it in the Galactic center.

The number of collisions per unit volume and time is given by

$$\frac{dn}{dt} = n_1 n_2 \Gamma \quad (7.2)$$

where  $n_1$  and  $n_2$  are the space densities of the two species of colliding stars. The rate coefficient for collisions among them in the limit where  $V \ll V_{\text{esc}}$  (Paper I) is given by

$$\Gamma = \langle \sigma_c V \rangle = \pi(R_1 + R_2)^2 \left[ \left( \frac{3}{\pi} \right)^{1/2} \left( \frac{V_{\text{esc}}^2}{\langle V^2 \rangle^{1/2}} \right) \right] \quad (7.3)$$

if their velocity dispersions are independent of their mass. Here  $\langle V^2 \rangle$  is the mean-squared velocity dispersion in the system. If we consider only collisions among a given species of stars, so  $n_1 = n_2 = n_0$ , then we replace  $n_1 n_2$  by  $(n_0^2)/2$  in equation (7.2) because each colliding star is counted twice in the summation leading to this equation. This equation must be integrated over the volume of the system to find the total rate of collisions per unit time. We shall now find this for globular clusters and the Galactic center.

#### i) Collisions in Globular Clusters

White dwarfs constitute  $\sim F_{\text{wd}} = 0.25$  of the mass of globular clusters (Hills 1978). We shall assume a similar mass fraction in the Galactic center. Hills and Day (1976) calculated the rate of collisions among stars in globular clusters by assuming that they consisted only of main-sequence stars with masses of  $0.4 M_{\odot}$  and radii of  $0.5 R_{\odot}$ . This gave an average of 335 collisions per globular cluster per Hubble time, which was based on the data for 41 globular clusters. The rate coefficient for collisions between white dwarfs with masses of  $0.6 M_{\odot}$  is  $\sim 0.038$  times that of these main-sequence stars. If 0.25 of the cluster mass is in white dwarfs, their collision rate is reduced by another factor of 16 compared to that calculated for main-sequence stars, so their collision rate is 0.0024 times that calculated for main-sequence stars or an average of 0.8 white dwarf collisions per globular cluster in the Galaxy. In the most favorable globular cluster, M80, about six to seven white dwarf collisions have occurred. A total of  $\sim 120$  white-dwarf collisions have occurred in the 150 globular clusters in the Galaxy. Most coalesced white dwarfs have masses below the Chandrasekhar limit, so after the collision they will remain as fast rotating, massive white dwarfs that will largely reside in the cores of the globular clusters. In this dense stellar environment, massive white dwarfs tend to accumulate in binaries by exchange collisions with existing binaries (Hills 1976).

#### ii) Collisions in the Galactic Center

The central core of the Galaxy provides an even more favorable environment for stellar collisions. Bailey (1980) finds that the stellar density at distance  $r$  from the Galactic center is about

$$\rho = \rho_c = 3 \times 10^7 M_{\odot}/\text{pc}^{-3}$$

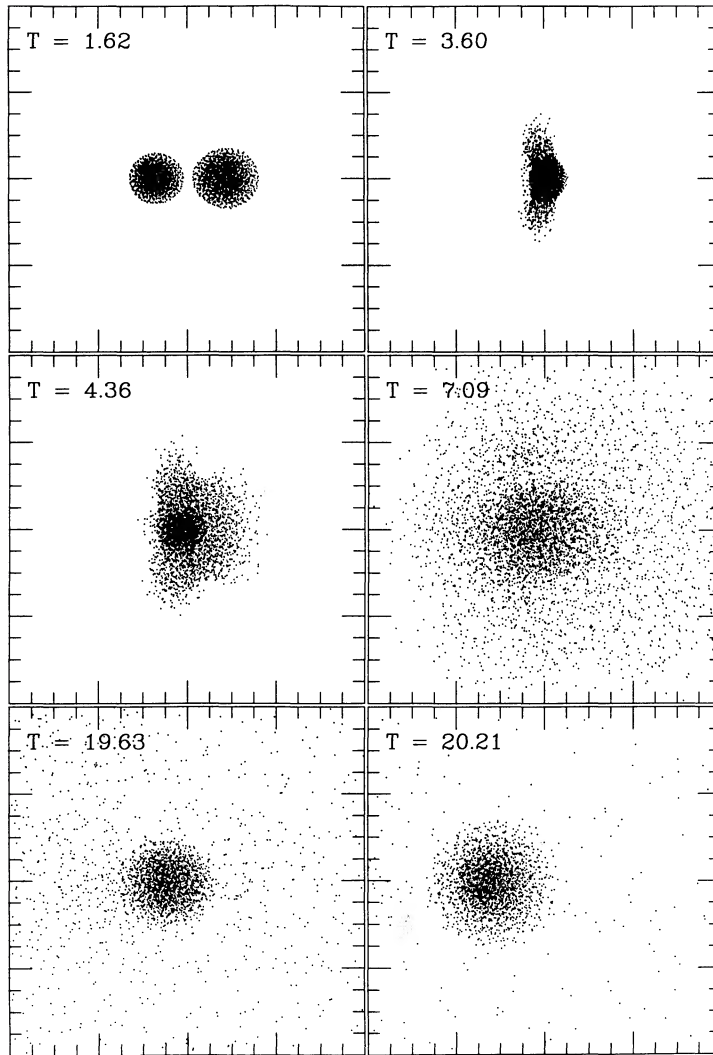


FIG. 12.—Projections onto the plane of the initial orbit of the velocity vectors of the fluid particles at various times during simulation 8, which shows a head-on collision between two white dwarfs with masses, of  $0. M_{\odot}$  and  $0.9 M_{\odot}$ . The times are given since the start of the simulation in seconds, and each frame covers an area of  $6.4 \times 10^9$  cm by  $6.4 \times 10^9$  cm.

for  $r < R_c = 0.1$  pc, while

$$\rho = \rho_c (r/R_c)^{-1.8}$$

for  $r = 0.1$ – $100$  pc. It is easy to show by integration that the total rate of stellar collisions outside the core radius,  $R_c$ , is just 5 times that within it so the total number of stellar collisions occurring per unit time in the Galactic center is 6 times that within  $R_c$ , or

$$\frac{dN}{dt} = 6 \left( \frac{4\pi}{3} \right) R_c^3 n_1 n_2 \Gamma, \quad (7.4)$$

where  $\Gamma$  is given by equation (7.3) and  $n_1 n_2$  is replaced by  $(n_0^2/2)$  if two colliding stars are identical.

If we assume that 0.25 of the mass of the Galactic core is in white dwarfs with masses of  $0.6 M_{\odot}$  and radii of  $0.0127 R_{\odot}$ , we find a collision occurs among these objects in the Galactic center about once every  $4 \times 10^6$  yr, so a total of 3000 white-dwarf collisions have occurred in the Galactic center in the past  $1.2 \times 10^{10}$  yr. If 0.125 of the stellar mass is composed of white dwarfs with masses of  $0.7 M_{\odot}$  and another 0.125 of the

mass is in white dwarfs with masses of  $0.9 M_{\odot}$ , then there were  $\sim 560$  collisions among the  $0.7 M_{\odot}$  white dwarfs, 350 collisions among the  $0.9 M_{\odot}$  white dwarfs, and  $\sim 960$  collisions between  $0.7 M_{\odot}$  and  $0.9 M_{\odot}$  white dwarfs for a total of 1870 collisions among all white dwarfs.

From Part I we find that in the limit where  $V \ll V_{\text{esc}}$ , the ratio of the mass-loss cross section to the coalescence cross section becomes

$$\frac{\sigma_{\text{ml}}}{\sigma_c} \rightarrow \int_0^{\infty} A \frac{dR_{\text{min}}}{(R_1 + R_2)}. \quad (7.5)$$

where  $A = \Delta M / (M_1 + M_2)$  is the fraction of the mass lost when the closest approach distance is  $R_{\text{min}}$ . These cross sections were found numerically from the data in Figures 1, 5, and 13. Figure 1 shows the integrated mass loss as a function of  $R_{\text{min}}$  for the two types of white-dwarf collisions while Figures 5 and 13 show the chemical composition of the ejected gas. Table 2 shows the computed mass-loss cross sections in units of the coalescence cross section.

We note that the integrated mass-loss cross section is  $\sim 3\%$  of the coalescence cross section for collisions between two  $0.6$

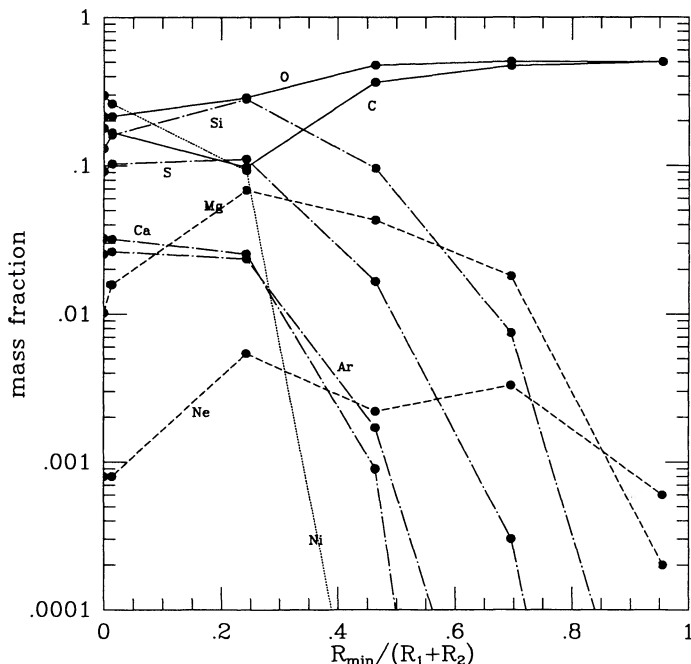


FIG. 13.—The fractional abundance of the chemical elements in the ejecta from collisions between a  $0.7 M_{\odot}$  white dwarf and a  $0.9 M_{\odot}$  one. These data are plotted as a function of the closest approach in the orbit in units of sum of the radii of the two white dwarfs.

$M_{\odot}$  white dwarfs and  $\sim 8\%$  for collisions between a  $0.7$  and a  $0.9 M_{\odot}$  white dwarf. All the ejected material is highly nuclear processed. If we assume that, on average, the mass-loss cross section is  $5.5\%$  for all white dwarfs and the average combined mass of two colliding white dwarfs is  $1.4 M_{\odot}$ , so  $\sim 0.08 M_{\odot}$  is

| Elements    | $0.6-0.6 M_{\odot}$  | $0.7-0.9 M_{\odot}$  |
|-------------|----------------------|----------------------|
| O .....     | $1.4 \times 10^{-2}$ | $2.6 \times 10^{-2}$ |
| C .....     | $1.3 \times 10^{-2}$ | $2.0 \times 10^{-2}$ |
| Si .....    | $1.5 \times 10^{-3}$ | $1.1 \times 10^{-2}$ |
| Ni .....    | $7.6 \times 10^{-4}$ | $1.2 \times 10^{-2}$ |
| S .....     | $6.6 \times 10^{-4}$ | $6.0 \times 10^{-3}$ |
| Mg .....    | $3.7 \times 10^{-4}$ | $1.9 \times 10^{-3}$ |
| Ne .....    | $2.2 \times 10^{-5}$ | $9.6 \times 10^{-5}$ |
| Ar .....    | $1.5 \times 10^{-4}$ | $1.4 \times 10^{-3}$ |
| Ca .....    | $1.6 \times 10^{-4}$ | $1.6 \times 10^{-3}$ |
| Total ..... | $3.1 \times 10^{-2}$ | $8.1 \times 10^{-2}$ |

ejected per coalescence, we find that for 2000 white-dwarf collisions in the Galactic center a total of  $\sim 60 M_{\odot}$  of processed material has been ejected into the interstellar medium. Assuming the average value given in the table, we see that as much as  $9\%$  of it may be radioactive nickel which ultimately decays into Fe. This corresponds to an average of  $0.01 M_{\odot}$  of Fe per collision, which is about an order of magnitude less than that ejected by SN 1987A. Collisions among white dwarfs are probably not serious competitors with supernovae in ejecting nuclear-processed elements into the interstellar medium, except, possibly for some trace elements.

One of us (W. B.) would like to thank the Theoretical Astrophysics Group, T-6, of the Los Alamos National Laboratory for their hospitality. Part of his work was supported by the Swiss National Science Foundation, and F.-K. T. acknowledges partial support from NSF grant AST 87-03535.

#### REFERENCES

- Bailey, M. E. 1980, *M.N.R.A.S.*, **190**, 217.  
 Benz, W. 1988, *Comput. Phys. Comm.* **48**, 97.  
 Benz, W., and Hills, J. G. 1987, *Ap. J.*, **323**, 628 (Paper I).  
 Benz, W., Bowers, R. L., Cameron, A. G. W., and Press, W. H. 1989, *Ap. J.*, in press.  
 Caughlan, G. R., Fowler, W. A., Harris, M. J., and Zimmermann, B. A. 1985, *Atomic Nucl. Data Tables*, **32**, 197.  
 Chandrasekhar, S. 1939, *Stellar Structure* (Chicago: University of Chicago Press).  
 Fowler, W. A., Caughlan, G. R., and Zimmerman, B. A. 1975, *Ann. Rev. Astr. Ap.*, **13**, 69.  
 Harris, M. J., Fowler, W. A., Caughlan, G. R., and Zimmerman, B. A. 1983, *Ann. Rev. Astr. Ap.*, **21**, 165.  
 Hills, J. G. 1976, *M.N.R.A.S.*, **175**, 1P.  
 ———. 1978, *Ap. J.*, **219**, 550.  
 Hills, J. G., and Day, C. A. 1976, *Ap. Letters*, **17**, 87.  
 Hulke, G., Rolfs, C., and Trautvetter, H. P. 1980, *Zs. Phys.*, **A297**, 161.  
 Itoh, N., Totsuji, H., Ichimaru, S., and De Witt, H. E. 1979, *Ap. J.*, **234**, 1079.  
 ———. 1980, *Ap. J.*, **239**, 415.  
 Monaghan, J. J. 1985, *Comput. Phys. Rep.*, **3**, 71.  
 Monaghan, J. J., and Lattanzio, J. C. 1985, *Astr. Ap.*, **149**, 135.  
 Nomoto, K., Thielemann, F.-K., and Miyaji, S. 1985, *Astr. Ap.*, **149**, 239.  
 Regev, O., and Shara, M. 1987, *M.N.R.A.S.*, **227**, 967.  
 Shara, M., and Shaviv, G. 1977, *M.N.R.A.S.*, **179**, 705.  
 ———. 1978, *M.N.R.A.S.*, **183**, 687.  
 Shara, M., and Regev, O. 1986, *Ap. J.*, **306**, 543.  
 Soker, N., Regev, O., Livio, M., and Shara, M. 1987, *Ap. J.*, **318**, 760.  
 Thielemann, F.-K., Arnould, M., and Truran, J. W. 1987, in *Advances in Nuclear Astrophysics*, ed. E. Vangioni-Flam et al. (Gif sur Yvette: Editions Frontieres), p. 525.  
 Thielemann, F.-K., and Truran, J. W. 1987, in *Advances in Nuclear Astrophysics*, ed. E. Vangioni-Flam et al. (Gif sur Yvette: Editions Frontieres), p. 541.

W. BENZ and F.-K. THIELEMANN: Harvard-Smithsonian Center for Astrophysics, 60 Garden Street, Cambridge, MA 02138

J. G. HILLS: Theoretical Division, T-6, MS B288, Los Alamos National Laboratory, Los Alamos, NM 87545